CWE-8
June 7-11, 2026
London, ON, Canada

Numerical Investigation of the Vertical Aerodynamic Forces Acting on a Bluff Body in a Tornado-like Flow

K. Uchiyama [a], T. Takeuchi [b], K. Nishijima [c]

[a]*Kobe University, Kobe, Hyogo, Japan, 255t019t@stu.kobe-u.ac.jp*
[b]*Kobe University, Kobe, Hyogo, Japan, takeuchi_t@person.kobe-u.ac.jp*
[c]*DPRI, Kyoto University, Uji, Kyoto, Japan, nishijima.kazuyoshi.5x@kyoto-u.ac.jp*

SUMMARY

This study investigates the vertical forces acting on a bluff body in a CFD-simulated tornado-like flow. The results show that significant upward forces act on objects positioned near the vortex center, driven by the pressure differential between the top and bottom surfaces. This force diminishes as the horizontal distance from the center increases. The upward force decreases as the height of the object increases; this occurs because the object becomes enclosed in the low-pressure core, reducing the pressure differential. This pressure reduction effect dominates the influence of the increased vertical drag. Objects with smaller footprints are more sensitive to the temporal deformation of the vortex core, causing large force fluctuations. In contrast, variations of the thickness of the object have a limited influence on the acting upward force.

Keywords: *Tornado-like flow, CFD, Vertical aerodynamic force, Bluff body, Core pressure deficit*

1. INTRODUCTION

Tornadoes generate intense horizontal winds capable of causing severe structural damage. However, field surveys have reported phenomena that are difficult to explain solely by the lift forces generated by horizontal wind, such as roof tiles being lofted and scattered, or vehicles being overturned. These observations suggest that substantial vertical upward forces act on objects during the approach of tornadoes. Previous studies have investigated the velocity and pressure fields of tornado-like flows using both experimental apparatuses and CFD simulations. Kikitsu et al. (2025) examined how swirl ratio and surface roughness density affect the velocity field and surface pressure deficit of tornado-like vortices, highlighting the gradual transition of the flow structure under varying parameters. Matsui et al. (2008) examined the velocity and pressure fields around a ground-mounted cube using a guide-vane type experimental apparatus, highlighting characteristic changes in wind pressure distribution depending on the presence of the cube. Ishihara et al. (2010) numerically modeled the experimental apparatus of Matsui et al. (2008) and validated its accuracy by comparing the results. They successfully generated tornado-like vortices with consistent shapes and velocities, and demonstrated that the updraft in a single-cell tornado-like vortex is driven by the vertical pressure gradient. Noda et al. (2018) developed a model capable of generating various types of tornado-like vortices within a simple rectangular computational domain, and proposed an approximate equation for the mean tangential velocity distribution. Maruyama (2010) demonstrated that tornadoes of single-cell, double-cell, and multiple-cell types, can be generated using a numerical model that omits guide vanes by combining free and Dirichlet boundary conditions. However, the vertical forces acting on specific objects within a vortex remain insufficiently understood. This is particularly true for scenarios where airflow can pass beneath the object, such as in the case of a vehicle.

In this study, a tornado-like flow is simulated using CFD to quantify the vertical forces acting on a bluff body placed within the vortex. Additionally, the effects of the object position and dimensions are investigated to account for the aerodynamic mechanisms governing the generation of these forces.

2. COMPUTATIONAL CONDITIONS

In this study, CFD simulations were performed using OpenFOAM v2206. The computational domain was constructed with reference to Maruyama (2010), as illustrated in Figure 1. An updraft was generated by applying a uniform outflow velocity of 1.0 m/s at the outlet located at the top of the convection region. Horizontal shear was introduced in the convergence region by setting up both inlets with a uniform inflow velocity of 0.5 m/s and openings with free inlet/outlet boundary conditions on portions of the side faces. These boundary conditions induced rotation within the convergence zone, forming a vortex. A no-slip condition was applied to the wall boundaries, and the pressure at the free inlet/outlet boundaries was set to zero. The Standard Smagorinsky model was utilized for Large Eddy Simulation (LES), with a total analysis time of 12 seconds.

Single box-shaped objects with varying dimensions were placed within the domain to analyze the acting vertical forces. The geometric parameters were defined as follows: D is the horizontal distance between the object center and the domain center; H is the height of the object center from the floor; L and T are the horizontal and vertical edge lengths of the object, respectively. Figures 2 and 3 show these four parameters in relation to the domain and the object. Analyses were conducted for Groups 1 to 4 (Table 1), varying these parameters to isolate their effects. The vertical force was evaluated using the wind force coefficient (C_z), defined as the resultant vertical force (F_z) acting on the top and bottom surfaces. C_z was calculated using Eq. (1).

$$C_z = \frac{F_z}{\frac{1}{2}\rho U^2 A} \tag{1}$$

The air density (ρ) was 1.2 kg/m³, and the reference area (A) was defined as the area of one face of the object ($A = L^2$). The reference wind speed (U) was defined as the maximum tangential velocity at the object center height for each simulation, ranging 2.30–3.15 m/s.

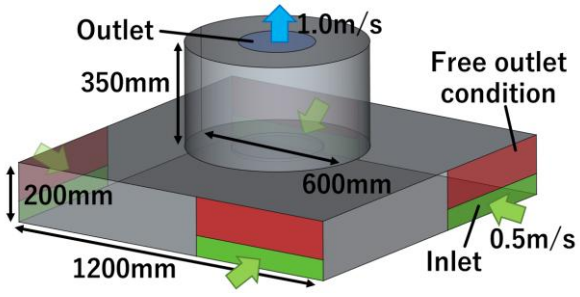

Figure 1: Analysis model.

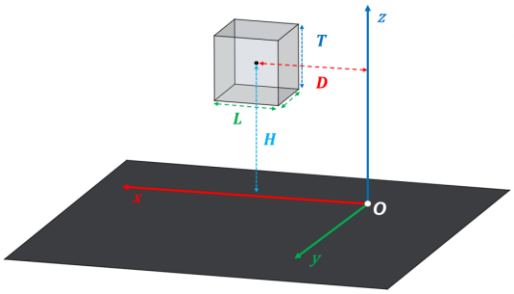

Figure 2: Changes in parameters of the object.

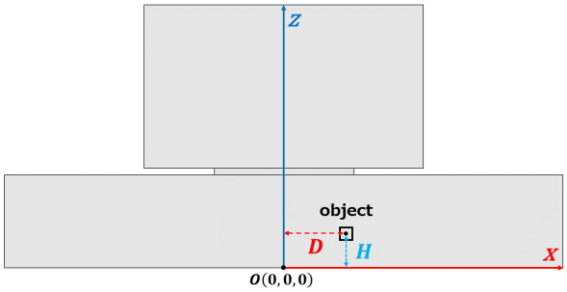

Figure 3: Cross-sectional view of the domain.

Table 1: Simulation cases and geometric parameters.

	D (mm)	H (mm)	L (mm)	T (mm)
Group 1	0, 20, 40, 60, 80, 100	30	20	
Group 2	0	30, 50, 70, 90	20	
Group 3	0	30	10, 20, 30	
Group 4	0	30	20	5, 10, 20

3. ANALYSIS RESULTS

3.1. Generated Vortex

In the absence of an object, a stable tornado-like vortex formed approximately 5–6 seconds after initialization. In a portion of the upper layer, vortex breakdown occurred, characterized by a downward flow at the center of the vortex. However, the flow almost entirely exhibits updrafts at the heights measured in this study.

Figure 4 shows the mean velocity vectors on the vertical cross section at the center of the computational domain, all of which are time-averaged over time t = 6 to 12 s, for the case where no object is placed in the flow, and the case of D = 0, 20 mm in Group 1, and H = 90 mm in Group 2. In addition, Figure 5 shows the mean vertical velocity $\overline{U}_z$ (over time 6 to 12 s) distributions along the x-axis at the center height of the object (in the case of no object, H = 30 mm). These results indicate that the mean vertical wind velocity near the object is upward in all cases, independent of the presence or location of the object. Consequently, the generated vortex is treated as a single-cell tornado-like vortex in the subsequent measurements. In the absence of an object, the generated vortex exhibited a core radius of 30 mm and a maximum tangential velocity of 2.64 m/s at a height of 30 mm.

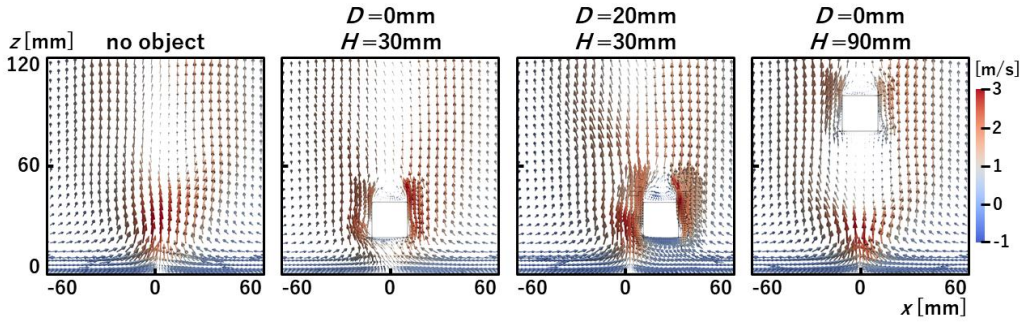

Figure 4: mean velocity vectors.

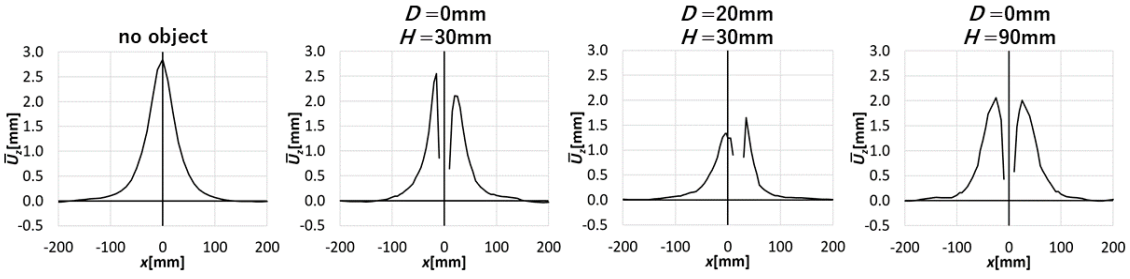

Figure 5: $\overline{U}_z$ distributions.

3.2. Effects of Horizontal Position (Group 1)

Figure 6 shows the time-averaged wind force coefficient $\overline{C_z}$ of the instantaneous wind force coefficient C_z (over time 6 to 12 s) for Groups 1 to 4. In Group 1, as the object horizontal position D increased, the value of $\overline{C_z}$ decreased. In addition, the time histories of the wind force coefficient C_z for Group 1 are shown in Figure 7. For D = 0 and 20 mm, strong vertical upward forces act on the object. However, for $D \geq 60$ mm, the wind force coefficient C_z becomes significantly smaller.

Figure 8 compares the vertical profiles of the time-averaged vertical velocity $\overline{U_z}$ and time-averaged static pressure $\overline{P}$ (over time 6 to 12 s) at the domain center for the case of D = 0 mm in Group1 and the case where no object is placed in the flow. In the absence of an object, an upward velocity of approximately 3.0 m/s is observed at a height of 20 mm. When the object is present, the maximum upward velocity beneath the object drops down to approximately 1.1 m/s, suggesting that drag due to the upward flow contributes less to the overall vertical force.

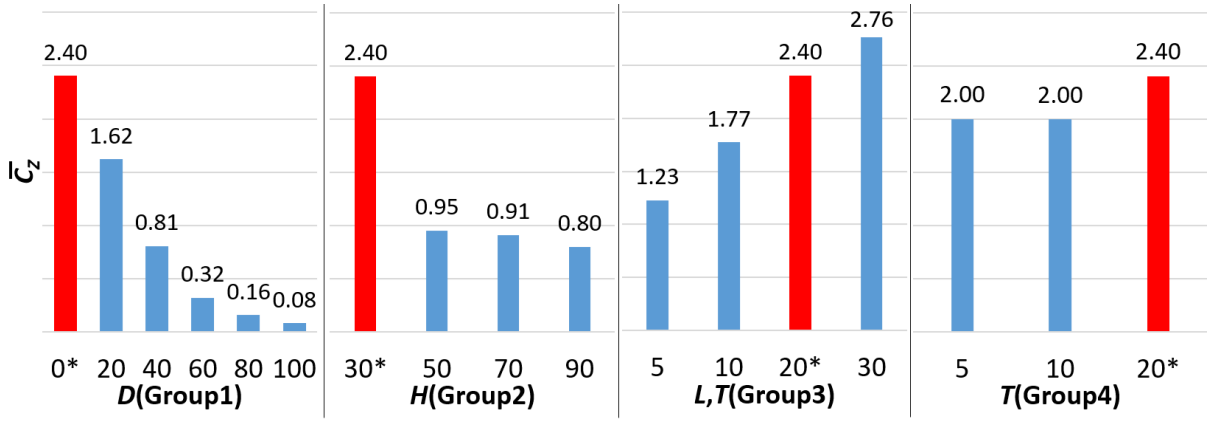

Figure 6: $\overline{C_z}$ for Groups 1 to 4 (time-averaged over 6-12 s)
(*the red bars represent the same reference value).

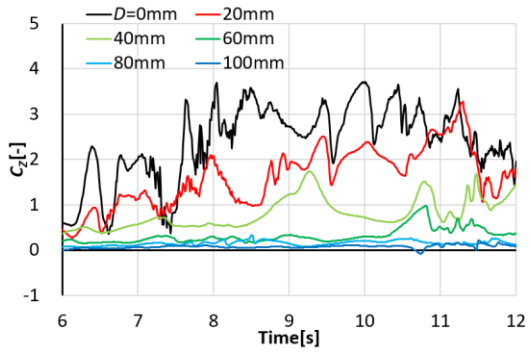

Figure 7: Time histories of C_z for Group 1 (varying D).

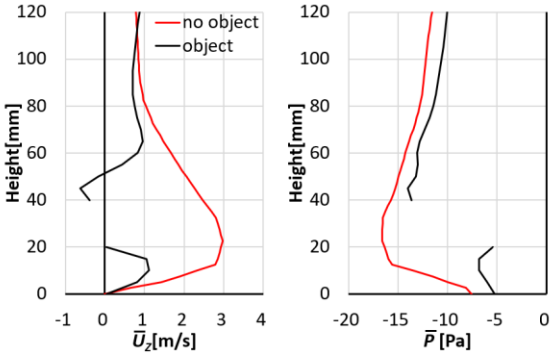

Figure 8: $\overline{U_z}$ and $\overline{P}$ profiles at center (No-object vs. D = 0 mm).

In contrast, the pressure differential between the top and bottom surfaces is significant. Figure 9 shows the time-averaged spatial pressure distributions (over time 6 to 12 s) on the cross section at the center of the computational domain. In the absence of an object, a distinct low-pressure region (blue) exists around the vortex center. On the other hand, for $D = 0$ and 20 mm, the low-pressure core does not seem to fully develop beneath the object, resulting in high pressure on the bottom surface of the object relative to the top surface. The resultant pressure differential is found to be the primary driver of the vertical upward force near the vortex center. Furthermore, for $D = 60$ mm, it is observed that the pressure difference between the top and bottom surfaces did not occur because the object was outside the low-pressure region; consequently, no vertical upward force was generated.

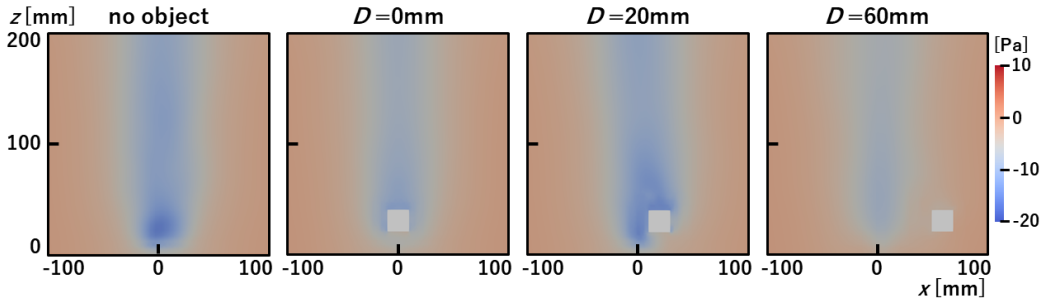

Figure 9: Mean pressure distributions.

3.3. Effects of Vertical Position (Group 2)

In Group 2, the height of the object center H varies. As shown in Figure 6, for $H \geq 50$ mm, the coefficient $\overline{C_z}$, and consequently the vertical force acting on the object, significantly decreases. To investigate the cause of the decrease, the time-averaged pressure distributions (over time 6 to 12 s) on the cross-section at the center of the computational domain for Group 2 are shown in Figure 10. From these figures it is observed that for $H = 30$ mm the low-pressure region of the vortex core is located only above the top surface of the object; in contrast, for $H \geq 50$ mm the object is completely enclosed in the low-pressure region. This enclosure significantly reduces the pressure differential between the top and bottom surfaces. Consequently, the net vertical upward force decreases.

This is further verified in Figure 11, which compares the vertical profiles of the time-averaged static pressure $\bar{P}$ on the object centerline, averaged between time $t = 6$ and 12 s, for the cases in Group 2. Whereas the pressure on the top surface shows little variation with H (ranging from -13.9 to -13.0 Pa), the pressure on the bottom surface at $H = 30$ mm (-5.4 Pa) is significantly higher than those in the cases of $H \geq 50$ mm (-10.7 to -9.9 Pa) . Consequently, the upward force is significantly greater for $H = 30$ mm.

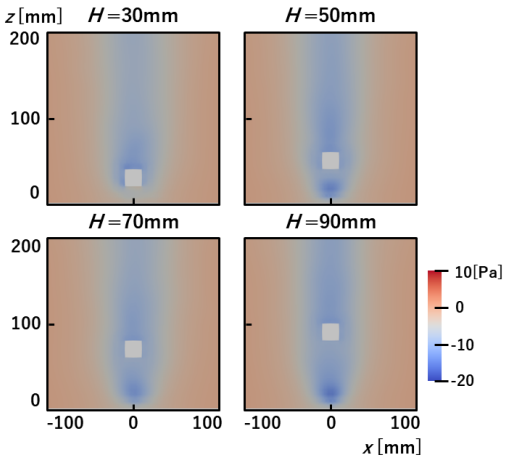

Figure 10: Mean pressure distributions for Group 2.

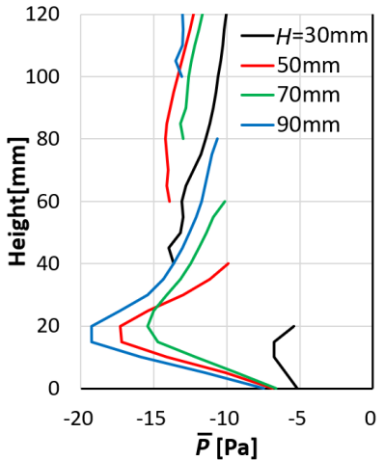

Figure 11: $\bar{P}$ profiles on the object centerline

3.4. Effects of Object Dimensions (Group 3)

In Group 3, the object dimensions L and T vary. As shown in Figure 6, small-sized objects tend to exhibit a lower time-averaged coefficient $\overline{C_z}$. Figure 12 shows the time history of C_z for the 5 mm and 30 mm cubic objects in Group 3. This figure indicates that a small-sized object results in an increase in the temporal fluctuations of C_z and a decrease in its mean value.

Figure 13 presents the instantaneous pressure distributions at 0.5 s intervals ranging from $t = 9.5$ s to 11.5 s. The 5-mm cubic object is small enough to be intermittently fully enclosed in the low-pressure region as the vortex deforms. For example, at $t = 10.5$ s, the cubic object is enclosed in the low-pressure region, resulting in a small vertical force, whereas at $t = 11.5$ s, a change in the vortex shape exposes the cube object to a pressure gradient, resulting in a larger vertical force. These results suggest that smaller objects are more sensitive to the temporal deformation of the vortex core, resulting in highly unsteady force coefficients. In contrast, larger objects are less sensitive to the fluctuations in the vortex structure; hence, they experience less fluctuation in the net pressure difference, resulting in a more stable wind force coefficient C_z.

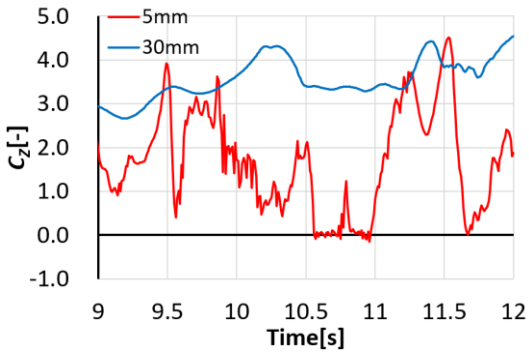

Figure 12: C_z histories for Group 3 (varying L, T).

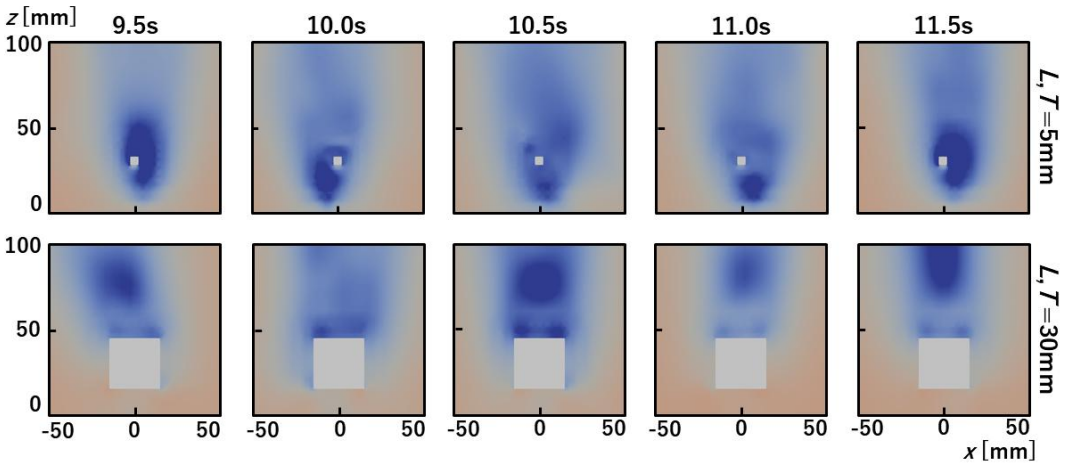

Figure 13: Instantaneous pressure distributions for 5 mm and 30 mm cubes.

3.5. Influence of Object Thickness (Group 4)

In Group 4, the vertical thickness T of the object varies. As indicated in Figure 6, little variation was observed in the pressure differential and the wind force coefficient. Figure 14 presents the time-averaged pressure distributions (over time 6 to 12 s) on the central cross-section of the computational domain for Group 4. These distributions indicate that there is no significant change in the pressure difference due to the thickness of the object. This, together with the previous observations, suggests that preventing the formation of a vortex core in the space beneath the object is the key factor in generating the large upward force.

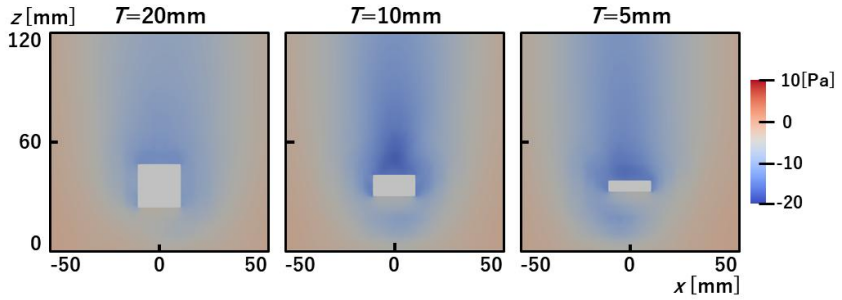

Figure 14: Mean pressure distributions for Group 4.

4. CONCLUSIONS

This study investigated the characteristics of the vertical force acting on a bluff body within a single-cell tornado-like flow by means of CFD simulations by varying the position and dimension of objects. The key findings are as follows:

(1) Significant vertical upward force acts on an object placed near the vortex center. This force is determined primarily by the pressure differential between the top and bottom surfaces. This force diminishes as the horizontal distance from the vortex center increases.

(2) The vertical upward force decreases as the object elevation increases.

(3) As the horizontal edge length of the object decreases, the object becomes more sensitive to the deformation of the vortex core. This sensitivity leads to large temporal fluctuations in the pressure difference and force coefficient due to the object being intermittently enclosed in the low-pressure region.

(4) Variations in the object's vertical thickness have a limited influence on the magnitude of the vertical upward force.

(5) The lack of vortex core formation between the object and the floor is the main cause of the upward force. This is particularly evident for larger objects or those located near the floor at the vortex core center.

ACKNOWLEDGEMENTS
This research was supported by JSPS KAKENHI Grant Number 24K01028.

REFERENCES

Ishihara et al., 2010. Numerical study on the flow field of tornado-like vortex using the LES turbulence model. The 21th National Symposium on Wind Engineering. 143-148. https://doi.org/10.14887/kazekosymp.21.0.143.0

Kikitsu et al., 2025. A study on structure of wind velocity distribution and corresponding pressure deficit characteristics under the tornado-like wind flow affected by surface roughness. J. Struct. Constr. Eng., AIJ, Vol.90, No.827. 15-26.

Maruyama T., 2010. Characteristics of numerically generated tornado-like vortex, DPRI annuals, No.53. 383-390.

Matsui et al., 2008. Wind pressure distribution around cube in tornadic flow and moving effects on tornadic flow, The 20th National Symposium on Wind Engineering. 319-324. https://doi.org/10.14887/kazekosymp.20.0.54.0

Noda et al., 2018. On distribution of mean tangential wind speed of tornado-like vortex, J. of Wind Engineering, JAWE, Vol.43, No.2(No.155). 48-55. https://doi.org/10.5359/jwe.43.48